Phonon Decoherence of Quantum Dots in Photonic Structures: Broadening of the Zero-Phonon Line and the Role of Dimensionality

P. Tighineanu,[1, *] C. L. Dreeßen,[1] C. Flindt,[2] P. Lodahl,[1] and A. S. Sørensen[1, †]

[1]*Niels Bohr Institute, University of Copenhagen,*
Blegdamsvej 17, DK-2100 Copenhagen, Denmark
[2]*Department of Applied Physics, Aalto University, 00076 Aalto, Finland*

We develop a general microscopic theory describing the phonon-induced decoherence of photons emitted by quantum dots placed in various photonic structures. The decoherence is found to depend fundamentally on the dimensionality of the structure resulting in vastly different performance for quantum dots embedded in a nano-cavity (0D), waveguide (1D), slab (2D), or bulk medium (3D). In bulk, we find a striking temperature dependence of the dephasing rate scaling as T^{11} implying that phonons are effectively 'frozen out' for $T \lesssim 4\,\mathrm{K}$. In photonic structures, the phonon density of states is strongly modified, which has a detrimental impact on the coherence properties. In particular for 1D and 2D structures, a linear temperature dependence is predicted for the decoherence, which can be important even at sub-Kelvin temperatures. Our findings provide a comprehensive understanding of the fundamental limits to photon coherence from quantum dots in photonic structures.

Disentangling a quantum system from its fluctuating environment is pivotal to the realization of coherent quantum bits. Controlling the sources of noise is particularly challenging in solid-state systems, which contain a myriad of mutually interacting quasi-particles. An example is semiconductor quantum dots (QDs), which have proven to be excellent solid-state quantum light sources that can be integrated into photonic devices [1]. Two important decoherence mechanisms of QDs are the fluctuating electrostatic [2, 3] and spin [2, 4, 5] environments but these can be neutralized under appropriate external control [6–9]. The decoherence is then dominated by the acoustic vibrations of the crystal lattice (phonons), which leads to a pronounced temperature dependence [10–14]. However, a unifying and comprehensive description of phonon decoherence in photonic structures is lacking despite its vital importance for solid-state quantum optics [1]. Previous founding work has concentrated on QDs in bulk media [11, 12] or the special case of linear phonon coupling in nano-wires [15] and carbon nanotubes [16]. Here we present a simple yet fully general microscopic theory of phonon decoherence that is applicable to explore the coherence of QD single-photon emission in any photonic (nano)structure, such as photonic-crystal cavities and waveguides, nano-beam waveguides, nano-wires, nano-diamonds, core-shell geometries, etc. The model is applied to the four experimentally relevant systems of an In(Ga)As QD in a cavity, waveguide, slab, or bulk medium corresponding to different geometric dimensionality from 0D to 3D, see Fig. 1(d).

The impact of phonons on the coherence of photon emission from QDs can be seen clearly in the emission spectrum [10–15, 17–27], which features broad spectral sidebands superimposed on a narrow emission line (known as the zero-phonon line or ZPL), cf. Fig. 1(a). The sidebands originate from a rapid phonon emission or absorption on a pico-second time scale, see Fig. 1(c), while the ZPL arises from the long-time decay of coherence over nano-second time scales. Due to the large spectral mismatch between the two processes, the sidebands can readily be removed by spectral filtering. The fundamental limit to photon coherence is therefore the interaction between the QD and phonons over long time scales, which is the main focus of the present Letter. In a bulk medium, the broadening is described by an exciton-phonon coupling that is quadratic in phonon displacement [11] corresponding to the scattering of a phonon, cf. Fig. 1(b). Here we show that a simple expression for the dephasing rate, Γ_{3D}, can be obtained by assuming that each phonon scatters from the QD a single time

$$\Gamma_{3D} = 3\pi C_Q^2 \int_0^\infty \mathrm{d}(qL)(qL)^{10}\mathrm{e}^{-(qL)^2}N_q(N_q+1),\qquad(1)$$

where C_Q is a constant defined later, L the QD radius, and q and N_q the phonon wavenumber and occupation number, respectively. Remarkably, when the thermal wavelength is larger than the QD size, $\lambda_{\mathrm{th}} > L$, corresponding to a temperature below a critical temperature $T_c = \hbar v_s/k_B L$ (v_s is the longitudinal speed of sound), the phonons responsible for the dephasing freeze out leading to a rapid drop of the dephasing rate, cf. Fig. 1(d). This yields $\Gamma_{3D}(T < T_c) \simeq 3\pi \times 10! \times C_Q^2(T/T_c)^{11}$ leading to highly coherent processes at $T \lesssim 4\,\mathrm{K}$ for realistic QD sizes. Nano-structures on the other hand are finite and can thus expand freely resulting in long-wavelength vibrations that broaden the ZPL already within the linear exciton-phonon coupling, see Fig. 1(c). The latter competes with the quadratic coupling to yield a non-trivial temperature dependence of the dephasing, cf. Fig. 1(d). We find that these processes severely limit the coherence in 1D and 2D photonic structures.
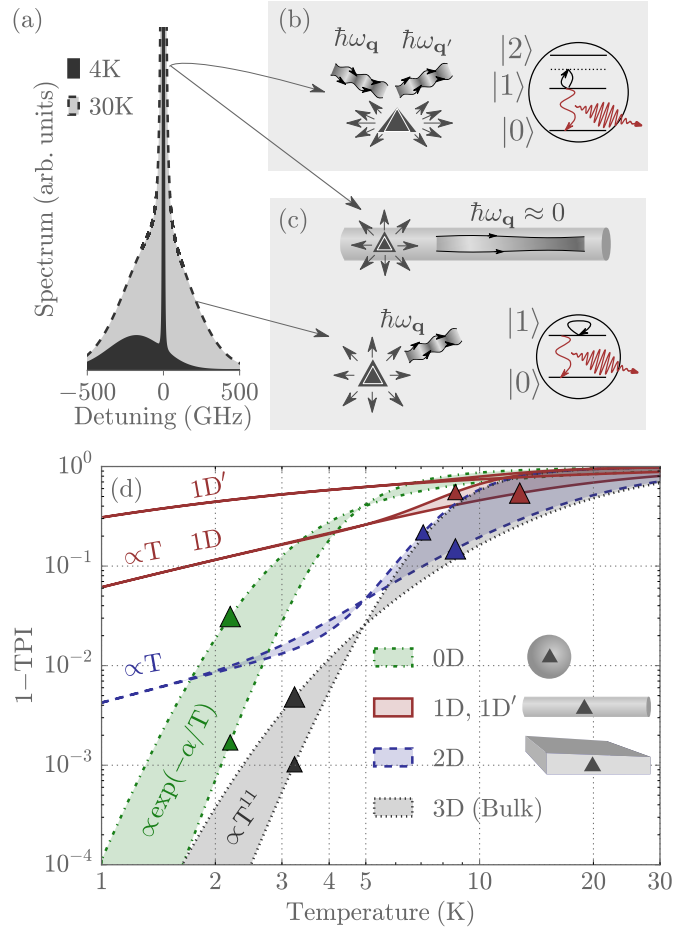
FIG. 1: Phonon dephasing of spontaneous emission from QDs. (a) The emission spectrum consists of a ZPL and broad sidebands. (b) The quadratic coupling represents scattering of phonons through virtual excitations to a higher lying state and leads to broadening of the ZPL. (c) The linear coupling is associated with the emission or absorption of phonons by the QD. In bulk this leads to phonon sidebands in the emission. In nano-structures (illustrated with a nano-wire), an additional mechanism broadens the ZPL through long-wavelength deformations. (d) Error in two-photon interference (1-TPI) versus temperature for QDs embedded in structures with different confining dimensionality. 0D corresponds to a QD in the center of a sphere with radius $R = 80\,\text{nm}$, 1D to a cylindrical waveguide with radius $\rho = 80\,\text{nm}$ and the QD placed in the cross-sectional center (1D) or halfway offcenter (1D'), 2D to a QD in the center of a freestanding membrane with height $2h = 160\,\text{nm}$, and 3D to a bulk medium. Each structure is represented by two curves that correspond to a large ($L = 4.5\,\text{nm}$) and small ($L = 1.5\,\text{nm}$) QD denoted with large and small triangles, respectively. The dephasing stemming from the linear coupling does not depend on L.

To derive our results we generalize the formalism developed in Ref. [11] and consider arbitrary photonic nano-structures with the following electron-phonon Hamiltonian

$$H = \hbar\omega_{01} |1\rangle \langle 1| + \sum_{\mathbf{q}} \hbar\omega_{\mathbf{q}} a_{\mathbf{q}}^{\dagger} a_{\mathbf{q}} + V_{\text{int}} |1\rangle \langle 1|, \tag{2}$$

where $|1\rangle$ is the QD excited state, $a_{\mathbf{q}}^{\dagger}$ ($a_{\mathbf{q}}$) the creation (annihilation) operator for the phonon mode with momentum $\mathbf{q}$ and energy $\hbar\omega_{\mathbf{q}}$, and $\hbar\omega_{01}$ is the QD transition energy, cf. Fig. 1(b). This Hamiltonian is based on the assumption that the thermal energy is small such that the QD excited states are not populated, which is a good assumption at cryogenic temperatures. The interaction term, $V_{\text{int}} = V_{\text{L}} + V_{\text{Q}}$, comprises a linear and a quadratic term in phonon

displacement

$$V_{\mathrm{L}} = \sum_{\mathbf{q}} L_{\mathbf{q}} A_{\mathbf{q}}, \quad V_{\mathrm{Q}} = \sum_{b,m} \left[\sum_{\mathbf{q}} Q_{\mathbf{q}b}^m A_{\mathbf{q}} \right]^2,$$

$$L_{\mathbf{q}} = M_{\mathbf{q}e}^{11} - M_{\mathbf{q}h}^{11}, \qquad Q_{\mathbf{q}b}^m = \frac{M_{\mathbf{q}b}^{1m}}{\sqrt{\Delta_m}}, \tag{3}$$

where $A_{\mathbf{q}} = a_{\mathbf{q}} + a_{\mathbf{q}}^\dagger$, $b = \{\mathrm{e,h}\}$ denotes electron or hole, $M_{\mathbf{q}b}^{mn}$ is the electron-phonon matrix element defined below, and Δ_m is the energy distance between the ground, $|1\rangle$, and m-th excited state of the QD with $m \geq 2$. Time-reversal symmetry is assumed such that all quantities can be chosen real. At low temperature, optical phonons do not play a role and we thus focus on the interaction with acoustic phonons. Two mechanisms dominate the electron-acoustic-phonon coupling: deformation-potential and piezo-electric coupling. The latter can be important for low-energy spin transfer [14] but is negligible in our case [28, 29]. We therefore consider a deformation-potential coupling of the form

$$M_{\mathbf{q}b}^{mn} = D_b \langle \psi_b^m | \nabla \cdot \mathbf{u_q} | \psi_b^n \rangle, \tag{4}$$

where D_b is the deformation-potential constant, ψ_b^m the wavefunction of the m-th excited state, and $\mathbf{u_q}$ the phonon displacement.

The coherence of the optical emission is described by the correlation function $P(t) = \mathrm{i} \langle \sigma^-(t)\sigma^+(0) \rangle = \mathrm{i} \left\langle \mathcal{T} \mathrm{e}^{-\frac{\mathrm{i}}{\hbar} \int_0^t \mathrm{d}\tau V_{\mathrm{int}}(\tau)} \right\rangle$ [11, 30], where $\mathcal{T}$ is the time-ordering operator. While it is possible to evaluate $P(t)$ exactly for a bulk medium [11], we follow a different path that simplifies the problem. We assume that each phonon only scatters a single time such that the influence of the QD on the phonon bath can be ignored as justified in Ref. [28]. In this case the phonon bath acts as an external Gaussian noise source. We define $F(t) = (1/\hbar) \int_0^t \mathrm{d}\tau V_{\mathrm{int}}(\tau)$ and thereby $P(t) \simeq \mathrm{i}\exp(-\mathrm{i}\mu_F) \exp\left[-\frac{1}{2}\left(\langle \mathcal{T} F^2(t) \rangle - \mu_F^2\right)\right]$, where $\mu_F = \langle F(t) \rangle$. Inserting Eq. (S5) into the above expression yields

$$P(t) = \mathrm{i} \exp\left[-\mathrm{i}\mu_F + K_{\mathrm{L}}(t) + K_{\mathrm{Q}}(t)\right],$$

$$K_{\mathrm{L}}(t) = -\frac{\mathrm{i}}{2\hbar} \sum_{\mathbf{q}} |L_{\mathbf{q}}|^2 \iint_0^t \mathrm{d}t \mathrm{d}t' D_{\mathbf{q}}(t-t'),$$

$$K_{\mathrm{Q}}(t) = \sum_{bmn} \iint_0^t \mathrm{d}t \mathrm{d}t' \left[\sum_{\mathbf{q}} Q_{\mathbf{q}b}^m Q_{\mathbf{q}b}^n D_{\mathbf{q}}(t-t') \right]^2, \tag{5}$$

where $D_{\mathbf{q}}(t) = (-\mathrm{i}/\hbar)\left[(N_{\mathbf{q}}+1)\mathrm{e}^{-\mathrm{i}\omega_{\mathbf{q}}|t|} + N_{\mathbf{q}}\mathrm{e}^{\mathrm{i}\omega_{\mathbf{q}}|t|}\right]$ is the phonon Green function. The function $K_{\mathrm{L}}(t)$ stems from the linear electron-phonon interaction and its magnitude is determined by a matrix element of the form $M_{\mathbf{q}b}^{11} \propto \langle \psi_b^1 | \nabla \cdot \mathbf{u_q} | \psi_b^1 \rangle$, which shares the symmetry of the ground-state wave function, implying that $K_{\mathrm{L}}(t)$ couples to symmetric acoustic deformations, cf. Fig. 1(c). On the other hand, $K_{\mathrm{Q}}(t)$ is mediated by acoustic deformations that share the symmetry of the excited m, n states.

In a bulk medium, the linear interaction $K_{\mathrm{L}}(t)$ gives a rapid decay of the coherence but does not contribute to its long-time decay, see Fig. 2(a). The quadratic polarization $|P_{\mathrm{Q}}(t)| = \exp[K_{\mathrm{Q}}(t)]$ is evaluated for a spherical QD with Gaussian envelopes of radius L. Since $K_{\mathrm{Q}}(t)$ is proportional to Δ_m^{-2}, the inclusion of the first triply degenerate excited state, $m = n = 2$, gives the dominant contribution. The imaginary part, $\mathrm{Im}[K_{\mathrm{Q}}(t)]$, is linear in time and only contributes to a spectral shift. Evaluating $P_{\mathrm{Q}}(t)$ numerically yields a Markovian decay over long time scales, cf. Fig. 2(a), with $\mathrm{Re}[K_{\mathrm{Q}}(t)] = -\Gamma_{\mathrm{3D}}t$, and can be calculated analytically by performing the time integration in Eq. (5) and using the long-time limit $\omega_{\mathbf{q}}^{-2}\sin^2\omega_{\mathbf{q}}t \simeq \pi t\delta(\omega_{\mathbf{q}})$. This leads to Eq. (1) with $C_{\mathrm{Q}} = \left(D_e^2/\Delta_e + D_h^2/\Delta_h\right)/3(2\pi)^2\rho_m v_s^2 L^3$. This is plotted in Fig. 2(b) for GaAs parameters: $v_s = 4780\,\mathrm{ms}^{-1}$, mass density $\rho_m = 5.37\,\mathrm{gcm}^{-3}$, $D_e = -14.6\,\mathrm{eV}$ and $D_h = -4.8\,\mathrm{eV}$ [15]. The energy distance to the excited states is taken to be $\Delta_e = 2\Delta_h = 40\,\mathrm{meV} \times L_0/L$ with $L_0 = 3\,\mathrm{nm}$, in agreement with theoretical estimates and experimental results [31–37].

Experimentally, the degree of coherence is measured in a Hong-Ou-Mandel setup [38], in which the two-photon indistinguishability, TPI, quantifies the coherence between two photons and ranges from 0 (no coherence) to 1 (full coherence). We calculate the TPI with the approach from Ref. [39] and obtain

$$\mathrm{TPI} = \Gamma_{\mathrm{rad}} \int_0^\infty \mathrm{d}\tau \mathrm{e}^{-\Gamma_{\mathrm{rad}}\tau} |P(\tau)|^2. \tag{6}$$

In bulk, $|P(t \gg t_0)| = \exp(-\Gamma_{\mathrm{3D}}t)$ leading to $\mathrm{TPI} = \Gamma_{\mathrm{rad}}/(\Gamma_{\mathrm{rad}} + 2\Gamma_{\mathrm{3D}})$ after filtering out the broad sidebands, where $\Gamma_{\mathrm{rad}} \simeq 1\,\mathrm{ns}^{-1}$ is the radiative decay rate of the QD [40], and $t_0 = L/v_s \sim 1\,\mathrm{ps}$. The resulting temperature
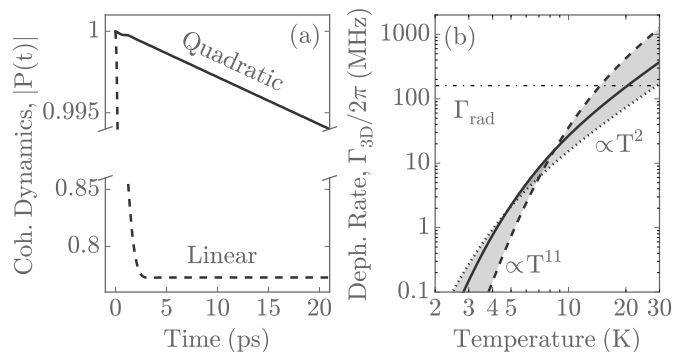
FIG. 2: Phonon dephasing in a bulk medium. (a) The linear exciton-phonon coupling causes a fast initial decay of the polarization, while the quadratic coupling contributes to the long-time decay. Parameters: $T = 10\,\mathrm{K}$, $L = 3\,\mathrm{nm}$. (b) Phonon dephasing rate versus temperature for $L = 1.5\,\mathrm{nm}$ (dashed line), $L = 3\,\mathrm{nm}$ (solid line) and $L = 4.5\,\mathrm{nm}$ (dotted line). The natural linewidth in a bulk medium, $\Gamma_{\mathrm{rad}} \simeq 2\pi \times 160\,\mathrm{MHz}$, is indicated by the dash-dotted line.

dependence of the TPI is plotted in Fig. 1(d). Near-unity indistinguishabilities, TPI $> 99\,\%$, can be achieved at temperatures below a few Kelvin, where the dephasing rate freezes out as T^{11}. The highly nonlinear temperature dependence leads to a significantly lower coherence at temperatures of 5–10 K. Analytic solutions can also be found at high temperatures, $\Gamma_{\mathrm{3D}}(T > T_c) \simeq 3 \times (105/32) \times \pi^{3/2} C_{\mathrm{Q}}^2 (T/T_c)^2$, with a quadratic dependence versus temperature as seen in Fig. 2(b).

The possibility to shape the photonic environment around the QDs with nano-structures has resulted in significant progress on controlling light-matter interactions [41–44]. Motivated by these achievements, we study phonon decoherence in nano-structures, where an additional source of decoherence is mediated by the linear exciton-phonon coupling owing to the modified density of states [15]. The long-time coherence dynamics can be split into two contributions $P_{\mathrm{ZPL}}(t) = P_{\mathrm{Q}}(t) P_{\mathrm{L0}}(t)$, where $P_{\mathrm{Q}}(t)$ stems from the quadratic coupling, and $P_{\mathrm{L0}}(t)$ is the nano-structure-specific low-frequency contribution to the linear coupling. We start with a simple example of a 0D system — a nano-sphere cavity, which resembles the geometry of colloidal QDs embedded in spherical shells [45]. The long-time coherence dynamics is plotted in Fig. 3(a) and stems solely from the quadratic coupling $P_{\mathrm{Q}}(t)$. The coherence decay is strongly non-Markovian because the phonons cannot escape and are reflected from the boundary of the sphere, thereby interacting with the QD periodically, see the inset of Fig. 3(a). A simple expression for $\mathrm{Re}\,[K_{\mathrm{Q}}(t)]$ can be derived from Eq. (5) by using the long-time form $\sin^2[(\omega_j - \omega_{j'})t]/(\omega_j - \omega_{j'})^2 \simeq t^2 \delta_{jj'}$, where j is the index of the confined acoustic mode. This results in $P_{\mathrm{ZPL}}(t) = \exp(-S^2 t^2)$ with

$$S^2 = \frac{3}{2}\left(\frac{\pi}{2}C_{\mathrm{Q}}\right)^2 \sum_j I_j^4 \tilde{q}_j^{12} e^{-\tilde{q}_j^2} N_{\tilde{q}_j}\left(N_{\tilde{q}_j} + 1\right), \tag{7}$$

where $\tilde{q}_j \equiv q_j L$, and I_j is a dimensionless normalization factor of the $(j,1,0)$ spheroidal mode [28, 46]. The resulting emission spectrum without the radiative broadening, $S(\omega) = \mathrm{Im}\int_0^\infty \mathrm{d}t P_{\mathrm{ZPL}}(t)\exp(-\mathrm{i}\omega t)$, is a Gaussian as depicted in Fig. 3(b). The TPI is evaluated with the help of Eq. (6) as $\mathrm{TPI}_{\mathrm{0D}} = \sqrt{\pi} r_{\mathrm{s}} \exp(r_{\mathrm{s}}^2)\mathrm{erfc}(r_{\mathrm{s}})$, where $r_{\mathrm{s}} = \Gamma_{\mathrm{rad}}/2\sqrt{2}S$, and is plotted in Fig. 1(d). In general, the decoherence is stronger than in bulk due to the enhanced correlation of the noise. In the small temperature limit $\lambda_{\mathrm{th}} \gg R$, the thermal energy becomes smaller than the lowest vibrational state of the sphere leading to negligible decoherence, $1 - \mathrm{TPI}_{\mathrm{0D}} \propto \exp(-\hbar\omega/2k_{\mathrm{B}}T)$, as depicted in Fig. 1(d).

In the following we discuss the dephasing of QDs embedded in 1D and 2D photonic structures, which are widely used in experiments as suspended 1D nanobeam waveguides [47], 1D nanowires [48], and suspended 2D photonic-crystal structures [41]. We find that the quadratic interaction does not deviate significantly from the case of a 3D medium because $K_{\mathrm{Q}}(t)$ is dominated by phonons with a wavelength comparable to the QD size. Realistic photonic structures are much larger than the QDs and thereby do not change the relevant phonon modes significantly. We therefore assume $K_{\mathrm{Q}}^{\mathrm{1D}} \simeq K_{\mathrm{Q}}^{\mathrm{2D}} \simeq -\Gamma_{\mathrm{3D}}t$ [28]. This is different for the linear interaction P_{L0} [15, 16]. For a freestanding 1D waveguide two families of acoustic modes contribute to dephasing with a finite $\nabla \cdot \mathbf{u}$: longitudinal expansions of the rod with a linear dispersion and thus a constant density of states at $\omega \to 0$, and flexural modes that bend the rod with a quadratic dispersion corresponding to a diverging density of states [28]. The former are purely longitudinal vibrations evenly distributed within the cross-sectional area [49], and yield a Markovian coherence decay that was found in Ref. [15] for a cylinder but here is generalized to an arbitrary cross-sectional shape and QD position with
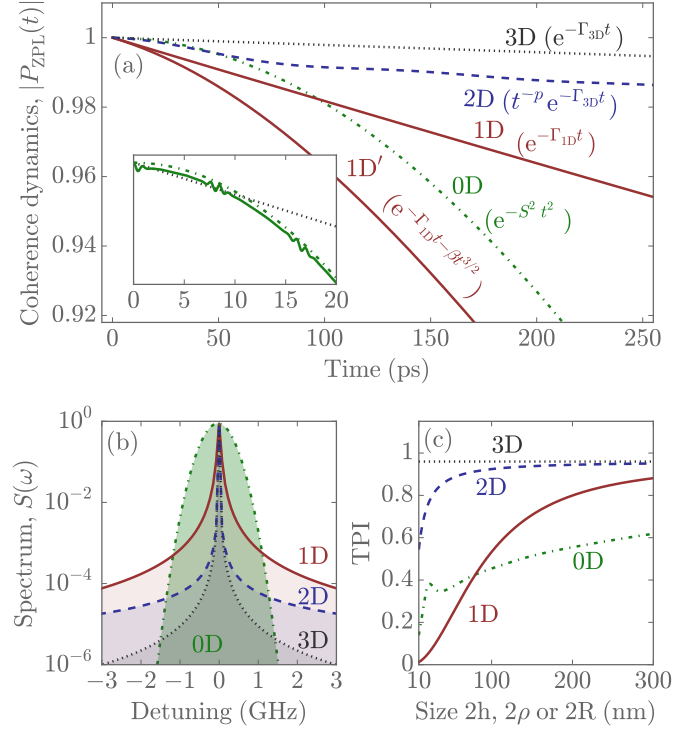
FIG. 3: Phonon dephasing in photonic structures and the role of dimensionality. (a) Decay of coherence for bulk (3D), a photonic membrane with $2h = 160\,\mathrm{nm}$ (2D), a photonic waveguide with $\rho = 80\,\mathrm{nm}$ with the QD position in the center (1D) and halfway offcenter (1D′), and a photonic sphere with $R = 20\,\mathrm{nm}$ (0D). Inset: initial decay of coherence (0–20 ps) for bulk (dotted line), sphere (solid line), and the t^2-approximation for the sphere (see text for details). (b) Corresponding emission spectrum for the cases of (a). (c) Two-photon indistinguishability versus size of the structure. All plots are for $T = 5\,\mathrm{K}$, $L = 3\,\mathrm{nm}$.

the rate

$$\Gamma_{\mathrm{L0}}^{\mathrm{1D}} = \frac{(D_e - D_h)^2 (1 - 2\nu)^2 k_{\mathrm{B}} T}{2 A \rho_m v_{\mathrm{1D}}^3 \hbar^2}, \tag{8}$$

where A is the cross-sectional area of the waveguide, $\nu = 0.299$ the GaAs Poisson ratio, and $v_{\mathrm{1D}} = v_s \sqrt{3 + 2\nu + 2/(\nu - 1)}$ the phonon speed along the waveguide axis. The total decay of coherence with the rate $\Gamma_{\mathrm{1D}} = \Gamma_{\mathrm{L0}}^{\mathrm{1D}} + \Gamma_{\mathrm{3D}}$ is plotted in Fig. 3(a). The coupling to flexural modes, on the other hand, strongly depends on the QD position, and ranges from no coupling at points of high symmetry (e.g., the center of a cylinder) to large coupling away from such points. In Fig. 3(a) we plot the numerically evaluated coherence decay of a QD placed halfway offcenter. The decay is non-Markovian scaling as $P_{\mathrm{1D'}} = e^{-\Gamma_{\mathrm{1D}} t - \beta t^{3/2}}$ [28]. In both cases, the decoherence scales as $\propto T$ at low temperatures and leads to a TPI that is significantly below unity even for diameters of hundreds of nanometers, see Fig. 1(d) and Fig. 3(c).

As an example of a 2D geometry we consider a QD embedded in a freestanding membrane with thickness $2h$. The fundamental vibrational mode associated with the expansion of the membrane [50] has a linear dispersion with $\omega = v_{\mathrm{2D}} q_{||}$, $v_{\mathrm{2D}} = v_s \sqrt{1 - 2\nu}/(1 - \nu)$, where $q_{||}$ is the in-plane wave number. The linear scaling of the density of states with ω therefore leads to

$$\mathrm{Re}\,[K_{\mathrm{2D}}] = -p \left[\gamma_{\mathrm{E}} + \int_{\frac{v_{\mathrm{2D}} t}{h}}^{\infty} \mathrm{d}\tau \frac{\cos\tau}{\tau} + \ln \frac{v_{\mathrm{2D}} t}{h} \right] - \Gamma_{\mathrm{3D}} t, \tag{9}$$

which is independent of the QD position; here, $p = (D_e - D_h)^2 (1 - 2\nu)^2 k_{\mathrm{B}} T / 4\pi \rho_m h v_{\mathrm{2D}}^4 (1 - \nu)^2 \hbar^2$, and γ_{E} is the Euler-Mascheroni constant. To obtain the above expression, we have approximated the dispersion of the fundamental mode as $\omega = v_{\mathrm{2D}} q_{||} \theta(h^{-1} - q_{||})$, which reproduces well the numerically exact solution [28], and θ is the Heaviside function. The coherence decay is plotted in Fig. 3(a) and results in a TPI that is dominated by the linear interaction at low temperatures as shown in Fig. 1(d). At long times ($t \gg h/v_{\mathrm{2D}}$), Eq. (9) can be simplified as

$P_{2D} = (v_{2D}t/h)^{-p}\exp(-\Gamma_{3D}t)$. QDs positioned away from the membrane center would also couple to flexural modes with quadratic dispersion resulting in a Markovian dephasing. Contrary to these examples, the 0D structure has a vanishing density of states at low frequencies. As used above, the dephasing is therefore only due to the quadratic coupling.

In conclusion, we have presented a simple framework for evaluating the phonon decoherence of photon emission from QDs. We find that the degree of confinement of the nano-structure has a significant impact on the degree of coherence, see Fig. 3(c). Bulk (3D) and maximally confined (0D) structures dephase the light-matter interaction solely due to the quadratic exciton-phonon coupling, which becomes negligible for $\lambda_{th} \gg L$ and $\lambda_{th} \gg R$, respectively. On the other hand, the coherence in 1D and 2D structures is limited by long-wavelength vibrations mediated by the linear exciton-phonon coupling. At low temperatures, the resulting degree of coherence scales linearly with temperature and sub-Kelvin temperatures may be required to neutralize them. Our study provides a quantitative foundation for calculating the impact of phonon dephasing in realistic photonic devices.

Acknowledgements

* Electronic address: petrut@nbi.ku.dk
† Electronic address: anders.sorensen@nbi.ku.dk

[1] Lodahl, P., Mahmoodian, S. & Stobbe, S. Interfacing single photons and single quantum dots with photonic nanostructures. *Rev. Mod. Phys.* **87**, 347 (2015).

[2] Kuhlmann, A. V. *et al.* Charge noise and spin noise in a semiconductor quantum device. *Nat. Phys.* **9**, 570 (2013).

[3] Arnold, C. *et al.* Cavity-Enhanced Real-Time Monitoring of Single-Charge Jumps at the Microsecond Time Scale. *Phys. Rev. X* **4**, 021004 (2014).

[4] Urbaszek, B. *et al.* Nuclear spin physics in quantum dots: An optical investigation. *Rev. Mod. Phys.* **85**, 79 (2013).

[5] Delteil, A., Gao, W.-b., Fallahi, P., Miguel-Sanchez, J. & Imamoğlu, A. Observation of Quantum Jumps of a Single Quantum Dot Spin Using Submicrosecond Single-Shot Optical Readout. *Phys. Rev. Lett.* **112**, 116802 (2014).

[6] Kuhlmann, A. V. *et al.* Transform-limited single photons from a single quantum dot. *Nat. Commun.* **6**, 8204 (2015).

[7] Somaschi, N. *et al.* Near-optimal single-photon sources in the solid state. *Nat. Photon.* **10**, 340 (2016).

[8] Ding, X. *et al.* On-demand single photons with high extraction efficiency and near-unity indistinguishability from a resonantly driven quantum dot in a micropillar. *Phys. Rev. Lett.* **116**, 020401 (2016).

[9] He, Y.-M. *et al.* On-demand semiconductor single-photon source with near-unity indistinguishability. *Nat. Nanotechnol.* **8**, 213 (2013).

[10] Besombes, L., Kheng, K., Marsal, L. & Mariette, H. Acoustic phonon broadening mechanism in single quantum dot emission. *Phys. Rev. B* **63**, 155307 (2001).

[11] Muljarov, E. A. & Zimmermann, R. Dephasing in Quantum Dots: Quadratic Coupling to Acoustic Phonons. *Phys. Rev. Lett.* **93**, 237401 (2004).

[12] Grange, T. Decoherence in quantum dots due to real and virtual transitions: A nonperturbative calculation. *Phys. Rev. B* **80**, 245310 (2009).

[13] Thoma, A. *et al.* Exploring Dephasing of a Solid-State Quantum Emitter via Time- and Temperature-Dependent Hong-Ou-Mandel Experiments. *Phys. Rev. Lett.* **116**, 033601 (2016).

[14] Zajac, J. M. & Erlingsson, S. I. Temperature dependency of resonance fluorescence from InAs/GaAs quantum dots: Dephasing mechanisms. *Phys. Rev. B* **94**, 035432 (2016).

[15] Lindwall, G., Wacker, A., Weber, C. & Knorr, A. Zero-Phonon Linewidth and Phonon Satellites in the Optical Absorption of Nanowire-Based Quantum Dots. *Phys. Rev. Lett.* **99**, 087401 (2007).

[16] Galland, C., Högele, A., Türeci, H. E. & Imamoğlu, A. Non-markovian decoherence of localized nanotube excitons by acoustic phonons. *Phys. Rev. Lett.* **101**, 067402 (2008).

[17] Muljarov, E. A., Takagahara, T. & Zimmermann, R. Phonon-Induced Exciton Dephasing in Quantum Dot Molecules. *Phys. Rev. Lett.* **95**, 177405 (2005).

[18] Kaer, P., Nielsen, T. R., Lodahl, P., Jauho, A.-P. & Mørk, J. Microscopic theory of phonon-induced effects on semiconductor quantum dot decay dynamics in cavity QED. *Phys. Rev. B* **86**, 085302 (2012).

[19] Madsen, K. H. *et al.* Measuring the effective phonon density of states of a quantum dot in cavity quantum electrodynamics. *Phys. Rev. B* **88**, 045316 (2013).

[20] Nazir, A. & McCutcheon, D. P. S. Modelling exciton-phonon interactions in optically driven quantum dots. *J. Phys.: Cond. Mat.* **28**, 103002 (2016).

[21] Borri, P. *et al.* Exciton dephasing via phonon interactions in InAs quantum dots: Dependence on quantum confinement. *Phys. Rev. B* **71**, 115328 (2005).

[22] Bayer, M. & Forchel, A. Temperature dependence of the exciton homogeneous linewidth in $In_{0.60}Ga_{0.40}As/GaAs$ self-assembled quantum dots. *Phys. Rev. B* **65**, 041308 (2002).

[23] Langbein, W. *et al.* Radiatively limited dephasing in InAs quantum dots. *Phys. Rev. B* **70**, 033301 (2004).

[24] Roy-Choudhury, K., Mann, N., Manson, R. & Hughes, S. Resonance fluorescence spectra from coherently driven quantum dots coupled to slow-light photonic crystal waveguides. *Phys. Rev. B* **93**, 245421 (2016).

[25] Roy-Choudhury, K. & Hughes, S. Quantum theory of the emission spectrum from quantum dots coupled to structured photonic reservoirs and acoustic phonons. *Phys. Rev. B* **92**, 205406 (2015).

[26] Kaer, P., Lodahl, P., Jauho, A.-P. & Mork, J. Microscopic theory of indistinguishable single-photon emission from a quantum dot coupled to a cavity: The role of non-Markovian phonon-induced decoherence. *Phys. Rev. B* **87**, 081308 (2013).

[27] Rudin, S., Reinecke, T. L. & Bayer, M. Temperature dependence of optical linewidth in single InAs quantum dots. *Phys. Rev. B* **74**, 161305 (2006).

[28] See Supplemental Material at [...] for further details.

[29] Takagahara, T. Theory of exciton dephasing in semiconductor quantum dots. *Phys. Rev. B* **60**, 2638 (1999).

[30] Mahan, G. D. *Many-particle physics* (Springer Science & Business Media, 2013).

[31] Schwartz, I. *et al.* Deterministic generation of a cluster state of entangled photons. *Science* aah4758 (2016).

[32] Pryor, C. Eight-band calculations of strained InAs/GaAs quantum dots compared with one-, four-, and six-band approximations. *Phys. Rev. B* **57**, 7190 (1998).

[33] Schmidt, K., Medeiros-Ribeiro, G., Oestreich, M. & Petroff, P. M. Excited states in inas self-assembled quantum dots. In *Photonics West*, 185 (International Society for Optics and Photonics, 1996).

[34] Noda, S., Abe, T. & Tamura, M. Mode assignment of excited states in self-assembled InAs/GaAs quantum dots. *Phys. Rev. B* **58**, 7181 (1998).

[35] Grundmann, M., Stier, O. & Bimberg, D. InAs/GaAs pyramidal quantum dots: Strain distribution, optical phonons, and electronic structure. *Phys. Rev. B* **52**, 11969 (1995).

[36] Landin, L., Miller, M., Pistol, M.-E., Pryor, C. & Samuelson, L. Optical studies of individual InAs quantum dots in GaAs: few-particle effects. *Science* **280**, 262 (1998).

[37] Stier, O., Grundmann, M. & Bimberg, D. Electronic and optical properties of strained quantum dots modeled by 8-band k·p theory. *Phys. Rev. B* **59**, 5688 (1999).

[38] Santori, C., Fattal, D., Vučković, J., Solomon, G. S. & Yamamoto, Y. Indistinguishable photons from a single-photon device. *Nature* **419**, 594 (2002).

[39] Kiraz, A., Atatüre, M. & Imamoğlu, A. Quantum-dot single-photon sources: Prospects for applications in linear optics quantum-information processing. *Phys. Rev. A* **69**, 032305 (2004).

[40] Johansen, J. *et al.* Size dependence of the wavefunction of self-assembled inas quantum dots from time-resolved optical measurements. *Phys. Rev. B* **77**, 073303 (2008).

[41] Arcari, M. *et al.* Near-unity coupling efficiency of a quantum emitter to a photonic crystal waveguide. *Phys. Rev. Lett.* **113**, 093603 (2014).

[42] Gazzano, O. *et al.* Bright solid-state sources of indistinguishable single photons. *Nat. Commun.* **4**, 1425 (2013).

[43] Madsen, K. H. *et al.* Efficient out-coupling of high-purity single photons from a coherent quantum dot in a photonic-crystal cavity. *Phys. Rev. B* **90**, 155303 (2014).

[44] Bennett, A. J. *et al.* Cavity-enhanced coherent light scattering from a quantum dot. *Science Advances* **2**, e1501256 (2016).

[45] Werschler, F. *et al.* Coupling of Excitons and Discrete Acoustic Phonons in Vibrationally Isolated Quantum Emitters. *Nano Lett.* **16**, 5861 (2016).

[46] Masumoto, Y. & Takagahara, T. *Semiconductor quantum dots: physics, spectroscopy and applications* (Springer Science & Business Media, 2013).

[47] Coles, R. *et al.* Chirality of nanophotonic waveguide with embedded quantum emitter for unidirectional spin transfer. *Nat. Commun.* **7** (2016).

[48] Heiss, M. *et al.* Self-assembled quantum dots in a nanowire system for quantum photonics. *Nat. Mater.* **12**, 439 (2013).

[49] Landau, L. & Lifshitz, E. *Theory of Elasticity (2nd ed.)* (Pergamon Press, 1970).

[50] Anghel, D. V. & Kühn, T. Quantization of the elastic modes in an isotropic plate. *J. Phys. A: Mathematical and Theoretical* **40**, 10429 (2007).

[51] Reigue, A. *et al.* Probing electron-phonon interaction through two-photon interference in resonantly driven quantum dots. *ArXiv* 1612.07121 (2016).

[52] Fry, P. W. *et al.* Inverted Electron-Hole Alignment in InAs-GaAs Self-Assembled Quantum Dots. *Phys. Rev. Lett.* **84**, 733 (2000).

[53] Skinner, J. L. & Hsu, D. Pure dephasing of a two-level system. *J. Phys. Chem.* **90** (1986).

[54] Kubo, R. Generalized cumulant expansion method. *J. Phys. Soc. Jpn.* **17**, 1100 (1962).

[55] Auld, B. A. *Acoustic fields and waves in solids* (John Wiley & Sons, 1973).

[56] Stroscio, M. A., Kim, K. W., Yu, S. & Ballato, A. Quantized acoustic phonon modes in quantum wires and quantum dots. *J. Appl. Phys.* **76**, 4670 (1994).

THEORY OF LINEAR AND QUADRATIC COUPLING TO ACOUSTIC PHONONS IN NANO-STRUCTURES

In this work we generalize the formalism presented in Ref. [11] to nano-structures and perform a key approximation, the single-scattering approximation, which we show below to be well justified for QDs and results in simple results. We also assume time-reversal symmetry, which implies that all the quantities (wave functions, phonon modes, etc.) can be chosen to be real. This means that the theory can be employed for single-particle excitations like excitons, trions, etc., as long as no fields or processes that destroy the time-reversal symmetry (e.g., magnetic fields) are present. We consider phonon processes that happen within the same spin manifold. This means that we neglect weak spin-flip processes between, e.g., bright-bright and bright-dark excitons.

We consider an exciton in a QD coupled to acoustic phonons with the following Hamiltonian [11]

$$
\begin{aligned}
H &= \sum_n E_n \left| \psi_n \right\rangle \left\langle \psi_n \right| + \sum_{\mathbf{q}} \hbar \omega_{\mathbf{q}} a_{\mathbf{q}}^\dagger a_{\mathbf{q}} + \sum_{nm} V \left| \psi_n \right\rangle \left\langle \psi_m \right|, \\
V &= \sum_{\mathbf{q}} L_{\mathbf{q}}^{nm} (a_{\mathbf{q}} + a_{\mathbf{q}}^\dagger),
\end{aligned}
\tag{S1}
$$

where the first two terms correspond to the bare Hamiltonians of the QD and the phonons, respectively, and the third term is the interaction Hamiltonian. Here, E_n is the energy of the n-th QD eigenstate ψ_n, $a_{\mathbf{q}}^\dagger$ ($a_{\mathbf{q}}$) is the creation (annihilation) operator of the phonon mode with wavevector $\mathbf{q}$ and energy $\hbar \omega_{\mathbf{q}}$, and $L_{\mathbf{q}}^{nm}$ is the effective electron-phonon matrix element. In writing the above equation, we have chosen the phase convention such that $L_{\mathbf{q}}^{nm}$ is real.

Two mechanisms dominate the interaction between electrons and acoustic phonons: deformation-potential and piezo-electric coupling [29]. The former describes the deformation of the lattice induced by the creation of an electron-hole pair inside the QD and has a matrix element of the form [29]

$$
L_{\mathbf{q},\mathrm{DF}}^{mn} = D_e \left\langle \psi_m \left| \nabla \cdot \mathbf{u}_{\mathbf{q}}(\mathbf{r}_e) \right| \psi_n \right\rangle - D_h \left\langle \psi_m \left| \nabla \cdot \mathbf{u}_{\mathbf{q}}(\mathbf{r}_h) \right| \psi_n \right\rangle,
\tag{S2}
$$

where $\mathbf{u}_{\mathbf{q}}$ is the phonon-displacement mode, and D_e (D_h) is the deformation-potential constant of electrons (holes). Equation (S2) describes the mechanical deformation of the crystal lattice induced by the creation of an electron-hole pair inside the QD. On the other hand, the piezo-electric coupling describes the interaction between the exciton and the polarization of the crystal lattice [29]

$$
L_{\mathbf{q},\mathrm{PZ}}^{mn} = \frac{2ep}{\epsilon_0 \epsilon} \hat{\mathbf{G}} \cdot \left(\left\langle \psi_m \left| \mathbf{u}_{\mathbf{q}}(\mathbf{r}_e) \right| \psi_n \right\rangle - \left\langle \psi_m \left| \mathbf{u}_{\mathbf{q}}(\mathbf{r}_h) \right| \psi_n \right\rangle \right),
\tag{S3}
$$

where $\epsilon_0 \epsilon$ (p) is the dielectric (piezo-electric) constant and $\hat{\mathbf{G}}$ is a geometric operator that is of the order of unity and depends on the symmetry of the acoustic deformation.

In the following we argue that the piezo-electric interaction is negligible in our study. Two types of phonons dephase the interaction between QDs and light in nano-structures: short-wavelength phonons of the order of the QD size $\lambda_{\mathrm{ph}} \sim L$, and long-wavelength phonons $\lambda \to \infty$ that arise in 1D and 2D structures. It is shown in Ref. [29] that the former dephase the QD mainly through the deformation-potential coupling with a negligible contribution from the piezo-electric coupling. To show that the latter is negligible also for long-wavelength deformations, we expand the mode displacement, $u_{\mathbf{q}} \propto \exp(\mathrm{i}\mathbf{q} \cdot \mathbf{r})$, in a Taylor series with respect to the electron (hole) center of mass, $\mathbf{r}_e$ ($\mathbf{r}_h$). Using Eqs. (S2) and (S3) this yields

$$
\left| \frac{L_{\mathbf{q},\mathrm{PZ}}^{11}}{L_{\mathbf{q},\mathrm{DF}}^{11}} \right|^2 \simeq \left| \frac{2ep}{\epsilon_0 \epsilon} \frac{\left\langle \psi_1 \left| \mathbf{r}_e - \mathbf{r}_h \right| \psi_1 \right\rangle}{D_e - D_h} \right|^2 \approx 10^{-2},
\tag{S4}
$$

where typical GaAs values were used $D_e = -14.6\,\mathrm{eV}$, $D_h = -4.8\,\mathrm{eV}$, $p = 0.16\,\mathrm{Cm}^2$, $\epsilon = 12.56$ [29], and a typical electron-hole separation of $\sim 0.4\,\mathrm{nm}$ in In(Ga)As QDs [52]. We have only considered the contribution to $L_{\mathbf{q}}^{11}$ because the other matrix elements are not relevant at small phonon energies as is shown later. We therefore neglect the piezo-electric coupling and consider $L_{\mathbf{q}}^{mn} \equiv L_{\mathbf{q},\mathrm{DF}}^{mn}$ in the following.

We assume that at $t = 0$ an exciton is created in the ground state $\left| \psi_1 \right\rangle$, and seek to calculate the evolution of the coherence $P(t) = i \left\langle \sigma^-(t) \sigma^+(0) \right\rangle$ at $t > 0$. Solving for $P(t)$ in the most general case with the Hamiltonian in Eq. (S1) is highly challenging. The problem can be simplified by noting that, at low temperature, only the ground state $\left| \psi_1 \right\rangle$

of the QD is populated. The excited states can then be eliminated as explained in Ref. [11], so that only virtual transition to excited states are taken into account. The resulting simplified Hamiltonian reads

$$H = H_0 + (V_{\mathrm{L}} + V_{\mathrm{Q}}) \, |\psi_1\rangle \langle \psi_1| \,,$$

$$V_{\mathrm{L}} = \sum_{\mathbf{q}} L_{\mathbf{q}} A_{\mathbf{q}}, \quad V_{\mathrm{Q}} = \sum_{b,m} \left[\sum_{\mathbf{q}} Q_{\mathbf{q}b}^m A_{\mathbf{q}} \right]^2,$$

$$L_{\mathbf{q}} \equiv L_{\mathbf{q}}^{11} = M_{\mathbf{q}e}^{11} - M_{\mathbf{q}h}^{11}, \qquad Q_{\mathbf{q}}^{mb} = \frac{M_{\mathbf{q}b}^{1m}}{\sqrt{\Delta_m}}, \tag{S5}$$

where $A_{\mathbf{q}} = a_{\mathbf{q}} + a_{\mathbf{q}}^\dagger$, $b = \{\mathrm{e}, \mathrm{h}\}$ denotes an electron or hole, $M_{\mathbf{q}b}^{mn} = D_b \langle \psi_{mb} | \nabla \cdot \mathbf{u_q} | \psi_{nb} \rangle$, and Δ_m is the energy distance between the ground, $|\psi_{1b}\rangle$, and m-th excited state of the QD, $|\psi_{mb}\rangle$. The Hamiltonian is now diagonal in the QD subspace but is quadratic in phonon displacement. Solving for $P(t)$ can be done using the cumulant expansion method presented in Refs. [11, 53] with the key difference that the phonon factorization used in those works does not hold in the case of a nano-structure. In the following we explain how to deal with this complication.

We start by writing $P(t)$ as [30]

$$P(t) = \mathrm{i} \left\langle \mathcal{T} \mathrm{e}^{-\frac{\mathrm{i}}{\hbar} \int_0^t \mathrm{d}\tau (V_{\mathrm{L}} + V_{\mathrm{Q}})} \right\rangle, \tag{S6}$$

where $\mathcal{T}$ denotes the time-ordering operator. Denoting $F(t) = -(\mathrm{i}/\hbar) \int_0^t \mathrm{d}\tau \, (V_{\mathrm{L}} + V_{\mathrm{Q}})$ and employing a well-known theorem for the cumulant [54] leads to

$$\begin{aligned} P(t) &= \mathrm{i} \exp \left\{ \sum_{n=1}^\infty \frac{1}{n!} \langle \mathcal{T} F^n(t) \rangle_{\mathrm{conn}} \right\} \\ &= \mathrm{i} \exp \left\{ \sum_{n=1}^\infty \left(\frac{-\mathrm{i}}{\hbar} \right)^n \frac{1}{n!} \int_0^t \mathrm{d}t_1 \int_0^t \mathrm{d}t_2 \ldots \int_0^t \mathrm{d}t_n \, \langle \mathcal{T} V(t_1) V(t_2) \ldots V(t_n) \rangle_{\mathrm{conn}} \right\}, \end{aligned} \tag{S7}$$

where $V = V_{\mathrm{L}} + V_{\mathrm{Q}}$, and the average operation is now performed over connected diagrams only. The linear, V_{L}, and quadratic, V_{Q}, terms contain matrix elements of different parity and thus do not mix allowing to express $P(t) = \mathrm{i} \exp \left[K_{\mathrm{L}}(t) + K_{\mathrm{Q}}(t) \right]$ with

$$K_{\mathrm{L}}(t) = \sum_{n=1}^\infty \left(\frac{-\mathrm{i}}{\hbar} \right)^n \frac{1}{n!} \int_0^t \mathrm{d}t_1 \int_0^t \mathrm{d}t_2 \ldots \int_0^t \mathrm{d}t_n \, \langle \mathcal{T} V_{\mathrm{L}}(t_1) V_{\mathrm{L}}(t_2) \ldots V_{\mathrm{L}}(t_n) \rangle_{\mathrm{conn}}, \tag{S8}$$

$$K_{\mathrm{Q}}(t) = \sum_{n=1}^\infty \left(\frac{-\mathrm{i}}{\hbar} \right)^n \frac{1}{n!} \int_0^t \mathrm{d}t_1 \int_0^t \mathrm{d}t_2 \ldots \int_0^t \mathrm{d}t_n \, \langle \mathcal{T} V_{\mathrm{Q}}(t_1) V_{\mathrm{Q}}(t_2) \ldots V_{\mathrm{Q}}(t_n) \rangle_{\mathrm{conn}}. \tag{S9}$$

It can be easily checked that the linear interaction contains only one connected diagram, $n = 2$, yielding

$$K_{\mathrm{L}}(t) = -\frac{\mathrm{i}}{2\hbar} \sum_{\mathbf{q}} |L_{\mathbf{q}}|^2 \iint_0^t \mathrm{d}t_1 \mathrm{d}t_2 D_{\mathbf{q}}(t_1 - t_2), \tag{S10}$$

$$D_{\mathbf{q}}(t) = -\frac{\mathrm{i}}{\hbar} \langle \mathcal{T} A_{\mathbf{q}}(t_1) A_{\mathbf{q}}(t_2) \rangle_{\mathrm{conn}} = -\frac{\mathrm{i}}{\hbar} \left[(N_{\mathbf{q}} + 1) \mathrm{e}^{-\mathrm{i}\omega_{\mathbf{q}}|t|} + N_{\mathbf{q}} \mathrm{e}^{\mathrm{i}\omega_{\mathbf{q}}|t|} \right], \tag{S11}$$

where $D_{\mathbf{q}}(t)$ is the phonon Green function [30]. Performing the time integration leads to

$$K_{\mathrm{L}}(t) = -\frac{1}{2\hbar^2} \sum_{\mathbf{q}} |L_{\mathbf{q}}|^2 \, d_{\mathbf{q}}(t), \tag{S12}$$

$$d_{\mathbf{q}}(t) = (2N_{\mathbf{q}} + 1) \left(\frac{\sin \frac{\omega_{\mathbf{q}} t}{2}}{\frac{\omega_{\mathbf{q}}}{2}} \right)^2 + \frac{2\mathrm{i}}{\omega_{\mathbf{q}}^2} \left(\sin \omega_{\mathbf{q}} t - 1 \right). \tag{S13}$$

This is the main result of the independent boson model [30] and is well known in the context of a bulk medium, where it leads to broad sidebands in the spectrum $S(\omega) = \mathrm{Im} \int_0^\infty \mathrm{d}t P(t) \exp(-\mathrm{i}\omega t)$. The linear cumulant contains a single propagator corresponding to the emission or absorption of a phonon, see Fig. S1(a).

The derivation of the quadratic cumulant, $K_Q(t)$, is more complicated and relies on a diagrammatic representation of the cumulant [53], which is outlined in the following. We drop the electron/hole index, b, to simplify the notation. We first note that the contribution from $n = 1$ to $K_Q(t)$ results in an irrelevant time-independent constant, $-i\mu_F$. Taking $n = 2$ gives two identical connected diagrams and yields

$$K_Q^{n=2}(t) = \sum_{m_1 m_2} \sum_{\mathbf{q_1}} Q_{\mathbf{q_1}}^{m_1} Q_{\mathbf{q_1}}^{m_2} \sum_{\mathbf{q_2}} Q_{\mathbf{q_2}}^{m_1} Q_{\mathbf{q_2}}^{m_2} \iint dt_1 dt_2 D_{\mathbf{q_1}}(t_1 - t_2) D_{\mathbf{q_2}}(t_2 - t_1)$$
$$= \sum_{m_1 m_2} \iint dt_1 dt_2 \left[Q_{\mathbf{q}}^{m_1} Q_{\mathbf{q}}^{m_2} D_{\mathbf{q}}(t_1 - t_2) \right]^2, \tag{S14}$$

which is equivalent to the third line of Eq. (5) in the main text. Generalizing this approach for $n = N$ can be done by identifying the number of equivalent connected diagrams [11, 53]. We thus obtain

$$K_Q(t) = \frac{1}{2} \sum_{n=2}^{\infty} \sum_{m_1 \dots m_n} \frac{1}{n} \iiint \dots \int dt_1 dt_2 \dots dt_n D_Q^{m_1 m_2}(t_1 - t_2) D_Q^{m_2 m_3}(t_2 - t_3) \dots D_Q^{m_n m_1}(t_n - t_1), \tag{S15}$$

$$D_Q^{mn}(t) = 2 \sum_{\mathbf{q}} Q_{\mathbf{q}}^m Q_{\mathbf{q}}^n D_{\mathbf{q}}(t). \tag{S16}$$

Equation (S15) is a generalization of the result from Ref. [11] for the case when no factorization with respect to the QD states can be performed. The quadratic cumulant contains an infinite sum of connected diagrams as illustrated in Fig. S1(b), and can be evaluated numerically at each time t using the Fredholm eigenvalue problem that is presented in Ref. [11]. However, we find that the interaction between QDs and phonons is sufficiently weak such that most of the physics is contained in the term $n = 2$ from Eq. (S14) as shown in the following.

BULK MEDIA (3D) AND THE SINGLE-SCATTERING APPROXIMATION

In the following we evaluate $P(t) = \exp(K_L(t) + K_Q(t))$ in a bulk medium. In this case the phonon modes are propagating plane waves, $\nabla \cdot \mathbf{u_q}(\mathbf{r}) = \sqrt{\hbar\omega_{\mathbf{q}}/2\rho_m v_s V} \exp(i\mathbf{q} \cdot \mathbf{r})$, where ρ_m is the mass density, v_s the longitudinal speed of sound, and V the quantization volume. We consider a spherical QD with parabolic confinement potential as explained in the main text. Plugging $\nabla \cdot \mathbf{u_q}$ into Eq. (S12) yields

$$K_L^{3D}(t) = -\frac{(D_c - D_v)^2}{8\pi^2 \hbar \rho_m v_s^3 L^2} \left\{ \int_0^{\infty} 2(1 + 2N_q) \left[1 - \cos(qLt/t_0)\right] (qL) e^{-(qL)^2/2} d(qL) - i\sqrt{2\pi} \frac{t}{t_0} \left(1 - e^{1-(t/t_0)^2/2}\right) \right\}, \tag{S17}$$

and the corresponding linear polarization is plotted in Fig. 2(a) in the main text.

To evaluate the quadratic interaction we consider the triply degenerate excited state only, $l = 1$ and $m = \{-1, 0, 1\}$, which is justified for thermal energies much smaller than the quantization energy. Then the quadratic cumulant, $K_Q(t)$, becomes diagonal in m in a bulk medium due to the spherical symmetry of the system and leads to

$$K_{Q,\text{sph}}(t) = \frac{3}{2} \sum_{n=2}^{\infty} \frac{1}{n} \iiint \dots \int dt_1 dt_2 \dots dt_n D_Q^{m_a m_a}(t_1 - t_2) D_Q^{m_a m_a}(t_2 - t_3) \dots D_Q^{m_a m_a}(t_n - t_1), \tag{S18}$$

where $D_Q^{m_a m_a}(t)$ denotes the quadratic propagator in which m_a can refer to any of the excited states $-1, 0, 1$. Here we are interested in the long-time decay of $P(t \gg t_0)$ with $t_0 = L/v_s$, i.e., the part responsible for the broadening of the zero-phonon line. Evaluating an exact-to-all-order expression for the long-time limit of $K_Q(t)$ is possible [53]. Here we discuss the simpler case of the single-scattering approximation in which the QD is assumed to interact with a phonon a single time during the scattering process, see Fig. S1(a). In other words, we only consider $n = 2$ and neglect the higher order diagrams. This yields

$$K_Q^{3D}(t) \simeq 3 \iint dt_1 dt_2 \left[\sum_{\mathbf{q}} Q_{\mathbf{q}}^{m_a} Q_{\mathbf{q}}^{m_a} D_{\mathbf{q}}(t_1 - t_2) \right]^2, \tag{S19}$$
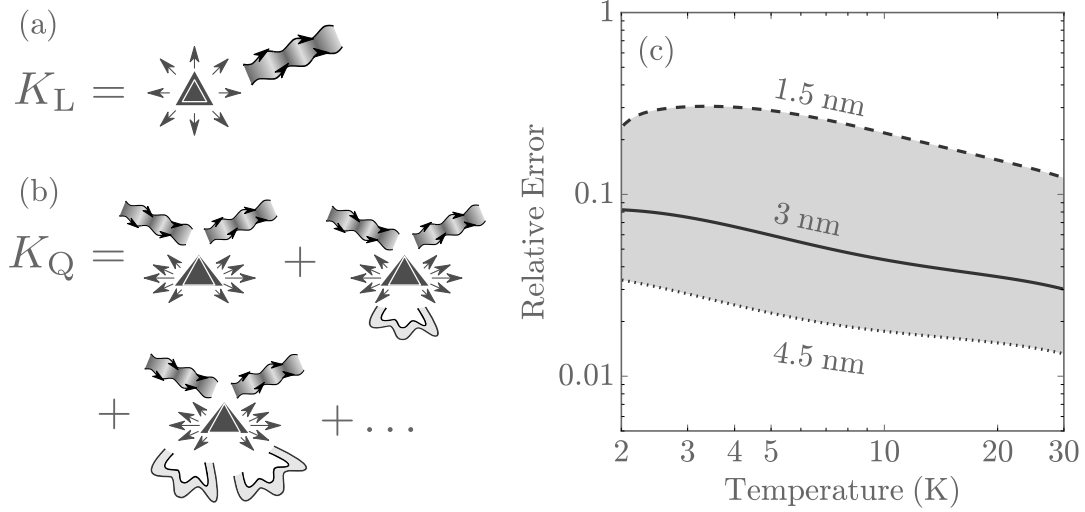
FIG. S1: (a) The linear cumulant contains a single electron-phonon interaction in the form of an emission or absorption process. (b) The quadratic cumulant contains an infinite series of scattering events. In the present paper we perform the single-scattering approximation meaning that only the first term on the right-hand side is retained. (c) The relative error in the decay rate, η, between the exact solution to the infinite series and the single-scattering approximation for $L = \{1.5\,\text{nm}, 3\,\text{nm}, 4.5\,\text{nm}\}$.

which can be evaluated by performing the integration over time

$$
\iint \mathrm{d}t_1 \mathrm{d}t_2 D_{\mathbf{q}_1}(t) D_{\mathbf{q}_2}(t) = -\frac{1}{\hbar^2} \left\{ (2N_{\mathbf{q}_1} N_{\mathbf{q}_2} + N_{\mathbf{q}_1} + N_{\mathbf{q}_2} + 1) \left[\frac{\sin\left(\frac{\omega_{\mathbf{q}_1} + \omega_{\mathbf{q}_2}}{2} t\right)}{\frac{\omega_{\mathbf{q}_1} + \omega_{\mathbf{q}_2}}{2}} \right]^2 \right.
$$
$$
\left. + (2N_{\mathbf{q}_1} N_{\mathbf{q}_2} + N_{\mathbf{q}_1} + N_{\mathbf{q}_2}) \left[\frac{\sin\left(\frac{\omega_{\mathbf{q}_1} - \omega_{\mathbf{q}_2}}{2} t\right)}{\frac{\omega_{\mathbf{q}_1} - \omega_{\mathbf{q}_2}}{2}} \right]^2 \right\}. \tag{S20}
$$

Using the long-time limit $\omega_{\mathbf{q}}^{-2} \sin^2 \omega_{\mathbf{q}} t \simeq \pi t \delta(\omega_{\mathbf{q}})$ results in a vanishing contribution from the first term on the right-hand side of Eq. (S20). We thus obtain $K_{\mathrm{Q}}^{\mathrm{3D}}(t) = -\Gamma_{3\mathrm{D}} t$ with

$$
\Gamma_{3\mathrm{D}} = 3\pi C_{\mathrm{Q}}^2 \int_0^\infty \mathrm{d}(qL)(qL)^{10} \mathrm{e}^{-(qL)^2} N_q(N_q + 1), \tag{S21}
$$

where $C_{\mathrm{Q}} = \left(D_e^2/\Delta_e + D_h^2/\Delta_h\right)/3(2\pi)^2 \rho_m v_s^2 L^3$. In bulk, the quadratic exciton-phonon interaction thus results in a Markovian decay of the coherence. The integrand contains an expression proportional to the squared joint phonon density of states, $q^{10} \exp(-q^2 L^2)$, multiplied by the phonon number, $N_q(N_q + 1)$, which is proportional to the probability to scatter a phonon because it involves a product of the number of incident phonons, N_q, and the rate of stimulated emission into a different mode of the same energy, $N_q + 1$.

The success of the single-scattering approximation is connected to the weak electron-phonon interaction in QDs, which means that the probability to interact multiple times with a phonon during a scattering event is negligible. To demonstrate this, we calculate the relative error

$$
\eta = \frac{|\Gamma_{3\mathrm{D}}^\infty - \Gamma_{3\mathrm{D}}|}{\Gamma_{3\mathrm{D}}^\infty}, \tag{S22}
$$

where $\Gamma_{3\mathrm{D}}^\infty$ is the dephasing rate that is exact to all orders, and is calculated with the help of Ref. [53]. Figure S1(c) plots η as a function of temperature for different QD sizes from which it can be inferred that the single-scattering approximation induces a relative error that is below $10\,\%$ for common QD sizes $L \sim 3\,\text{nm}$.

The single-scattering approximation is equivalent to the phonon bath acting as an external Gaussian noise source. To demonstrate this, we follow the derivation from the main text for $P(t)$, where we show that a classical noise source

results in a coherence function of the form

$$P(t) \simeq \mathrm{i} \exp(-\mathrm{i}\mu_F) \exp\left\{-\frac{1}{2}\left(\langle \mathcal{T}F^2(t)\rangle - \mu_F^2\right)\right\}, \tag{S23}$$

$$F(t) = (1/\hbar)\int_0^t \mathrm{d}\tau V(\tau). \tag{S24}$$

Inserting the interaction term, $V = V_{\mathrm{L}} + V_{\mathrm{Q}}$, into the above equation yields Eq. (S14). As opposed to the scattering description above, the expression in Eq. (S14) can thus also be seen as the result of the fluctuation in the potential induced by the thermal phonons. These fluctuations are proportional to the variance of the number of phonons in a thermal state, $N_q(N_q + 1)$.

MAXIMALLY CONFINED (0D) NANO-STRUCTURES

Here we derive the coherence function $P(t)$ for a QD placed at the center of a nano-sphere. The use of open boundary conditions at the surface of the nano-sphere (meaning that the force perpendicular to the surface must vanish so that the sphere vibrates freely) yields two classes of vibrational modes [46, 55]: torsional and spheroidal. The former are purely transversal and do not play a role for deformation-potential interactions. The spheroidal family of modes, $\mathbf{u}_{nlm}$, has three quantum numbers describing the vibrations along the radial direction, n, the total angular momentum of the mode, l, and its projection along the z-axis, m. The divergence of the spheroidal mode at the center of the sphere is

$$\nabla \cdot \mathbf{u}_{nlm}(\mathbf{r}) = -\mathcal{N}I_{nlm}q_n^2 j_l(q_n r) Y_{lm}(\Omega), \tag{S25}$$

where j_l is the spherical Bessel function of first kind and l-th order, Y_{lm} the spherical harmonic, Ω the solid angle, I_{nlm} the normalization constant of the mode, and $\mathcal{N} = \sqrt{\hbar/2\rho_m v_s}$. The linear cumulant is only mediated by modes with $l = m = 0$ because the linear exciton-phonon coupling is governed by a matrix element of the form $\langle \psi_{1b} | \nabla \cdot \mathbf{u}_{nlm} | \psi_{1b}\rangle$ with $\nabla \cdot \mathbf{u}_{nlm}$ given in Eq. (S25), and the ground-state exciton wavefunction, ψ_{1b}, is spherically symmetric. On the other hand, the quadratic cumulant is mediated by modes with $l = 1$, $m = \{-1, 0, 1\}$ because the quadratic exciton-phonon coupling is governed by a matrix element of the form $\langle \psi_{1b} | \nabla \cdot \mathbf{u}_{nlm} | \psi_{2b}\rangle$, and the excited state, ψ_{2b}, has the symmetry of a p orbital. The corresponding families of acoustic modes take the form

$$\mathbf{u}_{n00}(\mathbf{r}) = -\frac{\mathcal{N}}{2\sqrt{\pi}} I_{n00} j_1(q_n r)\hat{\mathbf{r}}, \tag{S26}$$

$$\mathbf{u}_{n1m}(\mathbf{r}) = \mathcal{N}\left\{I_{n1m}\nabla\Psi_{1m}(q_n\mathbf{r}) + J_{n1m}\nabla \times \nabla \times [\mathbf{r}\Psi_{1m}(k_n\mathbf{r})]\right\}, \tag{S27}$$

where $\Psi_{lm}(q\mathbf{r}) = j_l(qr)Y_{lm}(\Omega)$, $k_n = \sigma q_n$, $\sigma = v_s/v_t$ with v_t being the transverse speed of sound, and $\hat{\mathbf{r}}$ is the radial unit vector. I_{nlm} and J_{nlm} contain information about curl-free and divergence-free oscillations of the mode, respectively. Due to the rotational symmetry of the problem, the matrix elements with different angular momenta do not interfere in the quadratic cumulant, see Eq. (S14), resulting in a factorization similar to bulk. This means that it is sufficient to consider a single mode only and just to multiply its contribution by a factor of three. In the following we consider the state with $l = 1$ and $m = 0$. The normalization constants are found to be

$$I_{n00}^2 = \frac{4\tilde{q}_n}{2\left(\cos 2\tilde{q}_n + \tilde{q}_n^2 - 1\right) + \tilde{q}_n \sin 2\tilde{q}_n}, \tag{S28}$$

$$I_{n10}^2 = \frac{1}{L^2 + r_n^2 N^2 + 2r_n \mathrm{LN}}, \tag{S29}$$

$$L^2 = \frac{1}{4\tilde{q}_n^3}\left[-4 - 4\tilde{q}_n^2 + 2\tilde{q}_n^4 + 4(1 - \tilde{q}_n^2)\cos 2\tilde{q}_n + \tilde{q}_n(\tilde{q}_n^2 - 8)\sin 2\tilde{q}_n\right], \tag{S30}$$

$$N^2 = \frac{1}{\sigma^3 \tilde{k}_n^3}\left[-2 - 2\tilde{k}_n^2 + 2\tilde{k}_n^4 + 2(1 - \tilde{k}_n^2)\cos 2\tilde{k}_n + \tilde{k}_n(4 - \tilde{k}_n^2)\sin 2\tilde{k}_n\right], \tag{S31}$$

$$\mathrm{LN} = \frac{2}{\tilde{k}_n^3}\left(\tilde{q}_n\cos\tilde{q}_n - \sin\tilde{q}_n\right)\left(\tilde{k}_n\cos\tilde{k}_n - \sin\tilde{k}_n\right), \tag{S32}$$

where $\tilde{q} = qR$, and $r_n = J_{n10}/I_{n10}$. The vibrational eigenfrequencies and r_n are found from applying the open boundary conditions, which yields [46]

$$-\sigma^2 \tilde{q}_n j_0(\tilde{q}_j) + 4j_1(\tilde{q}_j) = 0 \text{ for } l = 0, \tag{S33}$$

$$\begin{pmatrix} \alpha_{nlm} & \beta_{nlm} \\ \gamma_{nlm} & \delta_{nlm} \end{pmatrix} \begin{pmatrix} I_{nlm} \\ J_{nlm} \end{pmatrix} = 0 \text{ for } l > 0, \tag{S34}$$

$$\alpha_{nlm} = -\sigma^2 \tilde{q}_n + 2(l+2)j_{l+1}(\tilde{q}_n), \tag{S35}$$

$$\beta_{nlm} = l\tilde{k}_n j_l(\tilde{k}_n) - 2l(l+2)j_{l+1}(\tilde{k}_n), \tag{S36}$$

$$\gamma_{nlm} = -\sigma^2 \tilde{q}_n j_l(\tilde{q}_n) + 2(l-1)j_{l-1}(\tilde{q}_n), \tag{S37}$$

$$\delta_{nlm} = (l+1)\left[2(l-1)j_{l-1}(\tilde{k}_n) - \tilde{k}_n j_l(\tilde{k}_n)\right]. \tag{S38}$$

These equations are solved numerically for each radial mode n.

The relevant electron-phonon matrix elements, $M_{\mathbf{q}b}^{11}$ and $M_{\mathbf{q}b}^{12}$, are evaluated for the vibrational mode $(n, l, 0)$ as

$$\left(M_{\mathbf{q}b}^{11}\right)_n = -D_b \frac{\mathcal{N}}{2\sqrt{\pi}} I_{n00} q_n^2 e^{-q_n^2 L^2/4}, \tag{S39}$$

$$\left(M_{\mathbf{q}b}^{12}\right)_n = -D_b \frac{\mathcal{N}}{2\sqrt{\pi}} I_{n10} \frac{q_n L}{\sqrt{6}} q_n^2 e^{-q_n^2 L^2/4}. \tag{S40}$$

This allows the computation of the linear and quadratic cumulants. The linear cumulant is evaluated using Eq. (S12) as

$$K_{\mathrm{L}}^{0\mathrm{D}}(t) = -\frac{(D_c - D_v)^2}{8\pi^2 \hbar \rho_m v_s^3 L^2} \frac{\pi}{2} \sum_n I_{00n}^2 (q_n L)^4 e^{-(q_n L)^2/2} \left[v_s^2 d_{q_n}(t)\right] \tag{S41}$$

This expression has a cutoff at wave numbers $q_n \gg L^{-1}$. It is therefore sufficient to evaluate the mechanical frequencies of the nano-sphere up to this cutoff only. We find numerically that the cumulant converges at $q_{\max} \simeq 5L^{-1}$. The same holds for the quadratic cumulant, which is discussed in the following.

The quadratic propagator is evaluated with the help of Eq. (S15) for the wavefunction with $l = 1, m = 0$ as

$$D_{\mathrm{Q}}(t) = \frac{\pi \hbar}{2} C_{\mathrm{Q}} \sum_n I_{n10}^2 q_n^6 e^{-(q_n L)^2/2} D_{q_n}(t). \tag{S42}$$

As mentioned above, the factorization of the angular momenta and the spherical symmetry result in the same contribution for the states with $l = 1, m = \pm 1$. The quadratic cumulant, $K_{\mathrm{Q}}(t)$, is evaluated numerically in Fig. 3(a) in the main text using the above expression and Eq. (S14), and compared to the t^2-approximation. The latter is calculated with the help of Eq. (S20) by employing the long-time limit $\sin^2[(\omega_n - \omega_{n'})t]/(\omega_n - \omega_{n'})^2 \simeq t^2 \delta_{nn'}$ yielding

$$K_{\mathrm{Q}}^{0\mathrm{D}}(t) = -S^2 t^2,$$
$$S^2 = \frac{3}{2} \left(\frac{\pi}{2} C_{\mathrm{Q}}\right)^2 \sum_n I_{n10}^4 (q_n L)^{12} e^{-(q_n L)^2} N_{q_n} (N_{q_n} + 1). \tag{S43}$$

The linear and quadratic polarizations along with the emission spectrum are plotted in Fig. S2. The linear polarization features an interference between the discrete modes of the sphere, which is reflected in the emission spectrum as detuned satellite peaks of the ZPL. Each spectral line is broadened by the quadratic exciton-phonon interaction, and is a Gaussian due to the t^2 dependence of the quadratic cumulant, see also Fig. 3 in the main text.

ONE-DIMENSIONAL (1D) NANO-STRUCTURES

Here we consider the phonon decoherence in realistic 1D photonic waveguides with any cross-sectional shape, which are relevant for various photonic platforms such as nano-wires and nano-beam waveguides.

The long-time decay of the polarization can be written as a product of a linear term, $P_{\mathrm{L0}}^{1\mathrm{D}}$, with low-frequency contributions from the linear exciton-phonon interaction, and a quadratic term, $P_{\mathrm{Q}}^{1\mathrm{D}}$, stemming from the quadratic exciton-phonon interaction, see main text for details. As argued in the main text, the quadratic polarization is
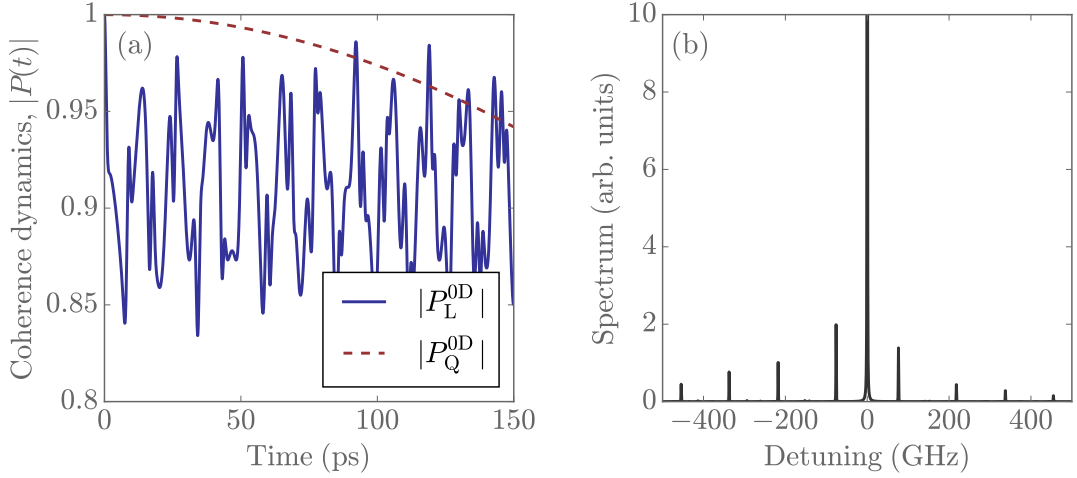
FIG. S2: (a) Coherence dynamics and (b) emission spectrum of a QD of $L = 3\,\mathrm{nm}$ embedded in a sphere of $R = 20\,\mathrm{nm}$ at $T = 5\,\mathrm{K}$. The spectrum features a ZPL and phonon replicas stemming from the linear exciton-phonon coupling. The lines are broadened by the quadratic electron-phonon coupling.

assumed to be the same as in bulk, $K_{\mathrm{Q}}^{\mathrm{1D}} = -\Gamma_{\mathrm{3D}}t$ due to the large mismatch between the size of the waveguide and of the QD. The evaluation of the linear polarization, $P_{\mathrm{L0}}^{\mathrm{1D}}$ is done as follows. Two families of acoustic modes are relevant with a finite $\nabla \cdot \mathbf{u}$: longitudinal modes in which the oscillations happen solely along the length, z, of the waveguide at low energies [56], and flexural modes that bend the waveguide [55]. The former are constant within the cross-section of a 1D waveguide [49] implying that the resulting decoherence is independent of the QD position. This results in a dephasing that depends solely on the cross-sectional area of the waveguide, and is independent of its shape. We thus evaluate the decoherence due to longitudinal modes for a cylindrical waveguide following Ref. [15] but note that the result is applicable to any cross-sectional shape with an equivalent area. The vibrational frequencies for a given wave vector $q_z \equiv q$ can be found from applying the traction-free boundary conditions at the surface of the cylinder and solving the corresponding characteristic equations [56]. The dispersion of the fundamental mode is found by expanding the characteristic equations in a Taylor series of $q_z \equiv q$ and retaining the lowest orders, which yields $\omega_q = v_{\mathrm{1D}}q$ with

$$v_{\mathrm{1D}} = v_s \sqrt{3 + 2\nu + \frac{2}{\nu - 1}}, \tag{S44}$$

where ν is the Poisson ratio. Expanding the displacement of the fundamental mode into a Taylor series and retaining the lowest order of q results in

$$u_r = \frac{\mathcal{N}_{\mathrm{cyl}}\nu}{\sqrt{\pi}\rho}r\sqrt{q}\mathrm{e}^{\mathrm{i}qz}, \tag{S45}$$

$$u_\phi = 0, \tag{S46}$$

$$u_z = \frac{\mathrm{i}\mathcal{N}_{\mathrm{cyl}}}{\sqrt{\pi}\rho}\frac{1}{\sqrt{q}}\mathrm{e}^{\mathrm{i}qz}, \tag{S47}$$

where r denotes the radial coordinate, ρ is the nanowire radius, and $\mathcal{N}_{\mathrm{cyl}} = \sqrt{\hbar/2\rho_m v_{\mathrm{1D}}A}$ with A being the cross-sectional area. The divergence of $\mathbf{u}$ is then to lowest order in q

$$\nabla \cdot \mathbf{u} = -\frac{\mathcal{N}_{\mathrm{cyl}}(1 - 2\nu)}{\sqrt{\pi}\rho}\sqrt{q}, \tag{S48}$$

and is independent of position as expected. The phonon number is large, $N_q \gg 1$, at such small vibrational frequencies compared to the thermal energy considered in this work. We can therefore expand N_q in a Taylor series and retain the lowest order in q, which is equivalent to the classical equipartition theorem yielding $N_q \hbar \omega_q = k_{\mathrm{B}}T$ in this case. It is worth noting that this expansion may not be valid at much smaller temperatures, a regime that is relevant for
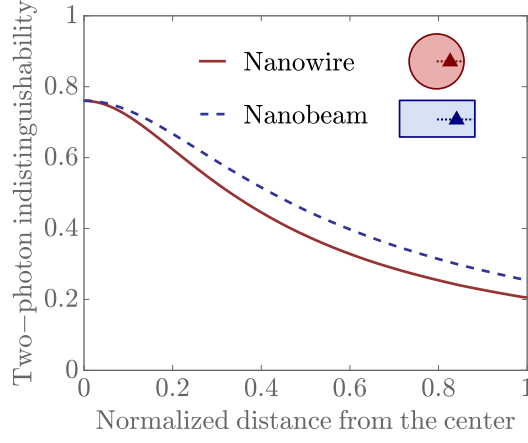
FIG. S3: Indistinguishability between two photons emitted by a QD embedded in a 1D waveguide versus the distance between the QD and the cross-sectional center of the waveguide. The plot shows two waveguides with an equivalent cross-sectional area: a nanowire with a radius of $80\,\text{nm}$ (solid red line), and a nanobeam of length $200\,\text{nm}$ and width $100\,\text{nm}$ (blue dashed line). At the center, only longitudinal modes contribute to the dephasing, and the TPI solely depends on the cross-sectional area and is therefore the same for the two waveguides. Away from the center, the QD also couples to flexural modes leading to a lower photon coherence. A temperature of $T = 5\,\text{K}$ was considered.

other systems such as carbon nano-tubes [16]. The real part of the linear cumulant can then be evaluated with the help of Eq. (S12) to yield to the lowest order in q

$$\text{Re}K_{\text{L0}}^{\text{1D}}(t) = -\frac{(D_e - D_h)^2(1 - 2\nu)^2}{4\pi\hbar^2\rho_m v_{\text{1D}}^2 A}k_\text{B}T \int_{-\infty}^{\infty} dq \left[\frac{\sin\left(\frac{\omega}{2}t\right)}{\frac{\omega}{2}}\right]^2 \simeq -\frac{(D_e - D_h)^2(1 - 2\nu)^2 k_\text{B}T}{2\hbar^2\rho_m v_{\text{1D}}^3 A}t = -\Gamma_{\text{L0}}^{\text{1D}}t, \qquad \text{(S49)}$$

where we have again assumed the long-time limit $\sin^2(\omega t)/\omega^2 \simeq \pi t\delta(\omega)$. The coherence decay stemming from longitudinal vibrations is therefore fully Markovian in a 1D structure with the rate $\Gamma_{\text{1D}} = \Gamma_{\text{3D}} + \Gamma_{\text{L0}}^{\text{1D}}$.

Away from the center of the nanowire, the QD is also dephased by flexural modes with a quadratic dispersion at low energies [49] resulting in a non-Markovian decay of coherence, see the main text for details. Figure S3 plots the numerically evaluated dephasing as a function of the QD position within the cross-section of a 1D waveguide. The dephasing due to flexural modes increases significantly as the QD approaches the edge of the waveguide. We have evaluated the decay of coherence due to flexural modes with a similar approach as for longitudinal modes from above, and found that the linear cumulant scales as $\text{Re}K_{\text{L0,flexural}}^{1D} = -\beta t^{3/2}$ with $\beta > 0$. The total decay of coherence for a QD positioned offcenter is thus $P_{\text{1D}'} = \exp(-\Gamma_{\text{L0}}^{\text{1D}}t - \beta t^{3/2})$, and is plotted in Fig. 3(a) in the main text.

TWO-DIMENSIONAL (2D) NANO-STRUCTURES

Here we evaluate the phonon decoherence of a QD placed in the center of a 2D photonic membrane of realistic thickness. Analogously to the 1D case, the long-time decay of the coherence, P_{ZPL}, is given by a product of the quadratic polarization, P_{Q}^{2D}, and the low-frequency contribution to the linear polarization, $P_{\text{L0}}^{\text{2D}}$. The latter is calculated similarly to the case of the cylinder by expanding the fundamental branch of the symmetric Lamb waves (all the other solutions are transverse at the QD position) into a Taylor series of the in-plane wave number $q_{||} \equiv q$. The dispersion is linear, $\omega = v_{\text{2D}}q$, which can be derived by solving the frequency equations [50] in the low-q and low-ω limits. The speed of sound in the plane of the membrane, v_{2D}, is found to be

$$v_{\text{2D}} = \frac{\sqrt{1 - 2\nu}}{1 - \nu}v_s. \qquad \text{(S50)}$$

The general analytic form of the displacement vector, $\mathbf{u} = u_{||}\hat{\mathbf{q}} + u_z\hat{\mathbf{z}}$ [50] (z points along the height of the membrane), is expanded in a Taylor series and normalized to one quantum of energy yielding to lowest order in q

$$u_{||} = \frac{\mathrm{i}\mathcal{N}_{\mathrm{m}}}{\sqrt{2}}\frac{1}{\sqrt{q}}\mathrm{e}^{\mathrm{i}\mathbf{q}\cdot\mathbf{r}_{||}}, \tag{S51}$$

$$u_z = \frac{\nu}{1-\nu}\frac{\mathcal{N}_{\mathrm{m}}}{\sqrt{2}}z\sqrt{q}\mathrm{e}^{\mathrm{i}\mathbf{q}\cdot\mathbf{r}_{||}}, \tag{S52}$$

where $\mathcal{N}_{\mathrm{m}} = \sqrt{\hbar/2\rho_m v_{\mathrm{2D}}}$. The divergence is thus

$$\nabla\cdot\mathbf{u} = -\frac{1-2\nu}{1-\nu}\frac{\mathcal{N}_{\mathrm{m}}}{\sqrt{2}}\sqrt{q}, \tag{S53}$$

and is again independent of position. Summing over q yields for the linear cumulant

$$\mathrm{Re}K_{\mathrm{L0}}^{\mathrm{2D}}(t) = -\frac{(D_e - D_h)^2(1-2\nu)^2 k_{\mathrm{B}}T}{8\pi\rho_m hv_{\mathrm{2D}}^4(1-\nu)^2\hbar^2}\int_0^\infty \omega\left[\frac{\sin\left(\frac{\omega t}{2}\right)}{\frac{\omega}{2}}\right]^2\mathrm{d}\omega. \tag{S54}$$

The integral on the right-hand side is diverging, which is caused by the artificial assumption that the dispersion is linear in the entire integration range. In reality, the dispersion becomes sublinear [50] resulting in a rapidly converging integral for $q \gtrsim h^{-1}$. To obtain an analytic expression, we make the following heuristic assumption for the dispersion, see Fig. S4(a)

$$\begin{aligned}\omega &= v_{\mathrm{2D}}q, & q &\le h^{-1}, \\ \omega &= 0, & q &> h^{-1}.\end{aligned} \tag{S55}$$

A qualitative justification for this assumption is that the acoustic waves become confined to the surface for q larger than h^{-1} [55] and do not interact with the QD. We thus obtain for the linear cumulant

$$\mathrm{Re}K_{\mathrm{L0}}^{\mathrm{2D}}(t) = -\frac{(D_e - D_h)^2(1-2\nu)^2 k_{\mathrm{B}}T}{4\pi\rho_m hv_{\mathrm{2D}}^4(1-\nu)^2\hbar^2}\left[\gamma_{\mathrm{E}} + \int_{\frac{v_{\mathrm{2D}}t}{h}}^\infty \mathrm{d}\tau\frac{\cos\tau}{\tau} + \ln\frac{v_{\mathrm{2D}}t}{h}\right], \tag{S56}$$

where γ_{E} is the Euler-Mascheroni constant. At times much larger than $t_{\mathrm{m}} = h/v_{\mathrm{2D}} \sim 20\,\mathrm{ps}$ for $h = 80\,\mathrm{nm}$, this expression is dominated by the last term, $\mathrm{Re}K_{\mathrm{L0}}^{\mathrm{2D}} \propto \ln(v_{\mathrm{2D}}t/h)$, which implies that the linear polarization decays polynomially with time, $P_{\mathrm{L0}}^{\mathrm{2D}}(t \gg t_{\mathrm{m}}) = (v_{\mathrm{h}}t/h)^{-p}$ with $p = 0.0085 \times T/1\,\mathrm{K}$ being the coefficient in front of the right-hand side of Eq. (S56). This analytic result is shown to reproduce qualitatively the numerically exact solution in Fig. S4(b). The temporal oscillations occurring with a period of $\sim t_{\mathrm{m}}$ are artifacts of the truncation: a stepwise truncation in the frequency domain results in a convolution with an oscillatory function in the time domain.

The quadratic polarization, $P_{\mathrm{Q}}^{\mathrm{2D}}$, is similar to the bulk value for realistic membrane thicknesses as argued in the main text. To demonstrate this quantitatively, we evaluate the quadratic cumulant in Eq. (S14) for a QD placed in the center of the membrane. All the modes up to $q = 5/L$ and $\omega/v_s = 5/L$ are evaluated numerically [50]. It is found that the propagators with different orbital symmetry do not interfere, $D_{\mathrm{Q}}^{mn} = D_{\mathrm{Q}}^{mn}\delta_{mn}$. This is due to the rotational symmetry around the z-axis meaning that the phonon modes can still be characterized by the angular momentum quantum number pointing along z. However, compared to bulk, the three terms are no longer equal: $D_{\mathrm{Q}}^{m=-1,n=-1} = D_{\mathrm{Q}}^{m=+1,n=+1} \ne D_{\mathrm{Q}}^{m=0,n=0}$, where in this case m and n denote the orbital angular momentum of the QD state. The terms $D_{\mathrm{Q}}^{m=n=\pm 1}$ are described by the interaction with symmetric (with respect to the center of the membrane) Lamb waves, $\mathbf{u}_s$, while $D_{\mathrm{Q}}^{m=n=0}$ is mediated by anti-symmetric vibrations, $\mathbf{u}_a$ [50]. The divergence of the modes is found to be

$$\nabla\cdot\mathbf{u}_s = -\mathcal{N}_{\mathrm{m}}N_s(q^2 + \alpha^2)A\cos(\alpha z)\mathrm{e}^{\mathrm{i}\mathbf{q}\cdot\mathbf{r}_{||}}, \tag{S57}$$

$$\nabla\cdot\mathbf{u}_a = \mathcal{N}_{\mathrm{m}}N_a(q^2 + \alpha^2)B\sin(\alpha z)\mathrm{e}^{\mathrm{i}\mathbf{q}\cdot\mathbf{r}_{||}}, \tag{S58}$$

where α and β are the transverse wavevectors subject to $\alpha^2 = \sqrt{\omega^2/v_s^2 - q^2}$ and $\beta^2 = \sqrt{\omega^2/v_t^2 - q^2}$, respectively, $A = 2\beta q\cos\beta$, $B = -2\beta q\sin\beta$, v_t is the transverse speed of sound, and N_s and N_a are normalization factors given in Ref. [50]. The electron-phonon matrix elements are evaluated as

$$M_{\mathbf{q}b}^{12\,m=\pm 1} = -D_b\mathcal{N}_{\mathrm{m}}\frac{\mathrm{i}}{\sqrt{2}}N_s AL(\pm q_x + \mathrm{i}q_y)(q^2 + \alpha^2)\mathrm{e}^{-(q^2 + \alpha^2)L^2/4}, \tag{S59}$$

$$M_{\mathbf{q}b}^{12\,m=0} = D_b\mathcal{N}_{\mathrm{m}}\frac{1}{\sqrt{2}}N_a BL\alpha(q^2 + \alpha^2)\mathrm{e}^{-(q^2 + \alpha^2)L^2/4}. \tag{S60}$$
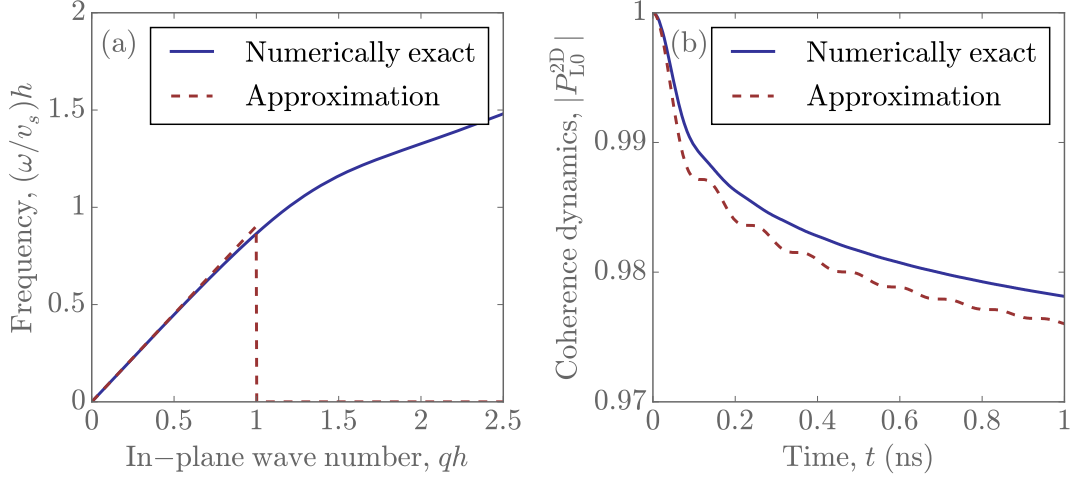
FIG. S4: Impact of the approximation performed in Eq. (S55). Parameters: $L = 3\,\text{nm}$, $T = 10\,\text{K}$. (a) Graphical illustration of the approximation. The numerically exact dispersion is replaced by a linear function with a cutoff at $qh = 1$. (b) The approximation allows to obtain an analytic expression for the coherence dynamics, which reproduces with reasonable accuracy the numerically exact solution.
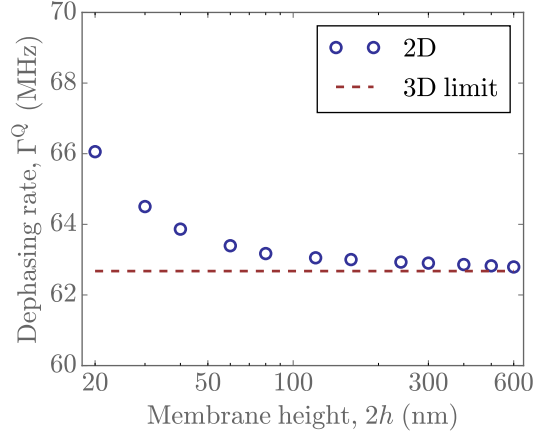
FIG. S5: Dephasing due to the quadratic exciton-phonon interaction for a 2D membrane. The rate is found to rapidly converge to the 3D value for realistic membrane thicknesses. Parameters: $L = 3\,\text{nm}$, $T = 10\,\text{K}$.

The propagators are therefore found to be

$$D_{\text{Q}}^{m=n=\pm 1} = \frac{3\pi h}{L} C_Q \sum_\alpha \int_0^\infty q^3(\alpha^2 + q^2)^{3/2} |N_s|^2 \, e^{-(q^2+\alpha^2)/2} \hbar D_{\mathbf{q}}(t) \mathrm{d}q \tag{S61}$$

$$D_{\text{Q}}^{m=n=0} = \frac{6\pi h}{L} C_Q \sum_\alpha \int_0^\infty q\alpha^2(\alpha^2 + q^2)^{3/2} |N_a|^2 \, e^{-(q^2+\alpha^2)/2} \hbar D_{\mathbf{q}}(t) \mathrm{d}q \tag{S62}$$

The resulting decay rate is found to be Markovian with the rate $\Gamma_{\text{2D}}^{\text{Q}}$, which is compared to the bulk value, Γ_{3D}, in Fig. S5 as a function of membrane thickness. The 2D rate is very close to the bulk limit for realistic membrane thicknesses, which is why the quadratic interaction is assumed to be bulk-like throughout the main text.